Reliability Engineering and System Safety 244 (2024) 109910

Contents lists available at ScienceDirect

Reliability Engineering and System Safety

journal homepage: www.elsevier.com/locate/ress

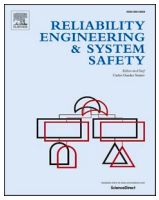

Looking beyond individual failures: A system-wide assessment of water infrastructure resilience to extreme events

Helena R. Tiedmann, Kasey M. Faust, Lina Sela *

Fariborz Maseeh Department of Civil, Architectural and Environmental Engineering, The University of Texas at Austin, 301 Dean Keeton St. C1752, Austin, TX 78712, USA

ARTICLE INFO

Keywords:
Water infrastructure
Resilience
Extreme events
Pipe failures
Network structure
Spatial cluster analysis

ABSTRACT

Water infrastructure systems throughout the United States face compounding challenges due to aging infrastructure and increasingly extreme and more frequent weather events. Identifying vulnerabilities and assessing systems' ability to withstand and recover from such events is a critical component of water infrastructure planning and management. Pipe failures and system structure can substantially impact water infrastructure resilience, but these two factors are often assessed separately. Here, we present a holistic assessment of system performance that considers pipe failures, active water storage, and system structure utilizing data collected during normal and emergency operating conditions. The four-step framework evaluates pipe failures spatially and temporally to assess overall system performance, as measured by active storage, and identifies targeted areas for improvements. Employing control charts, resilience curves, and spatial clustering analysis, our results simultaneously reveal an agreement between trends in pipe failures during normal and emergency operating conditions as well as unexpected discrepancies between pipe failures and system performance due to the water system structure. Our results offer insights to utilities seeking to assess system vulnerabilities to increase water infrastructure resilience to extreme events.

1. Introduction

As infrastructure assets throughout the United States (U.S.) approach the end of their service life, many water infrastructure systems are increasingly operating outside of the conditions for which they were designed. In 2021, U.S. drinking water infrastructure scored a C- on America's Infrastructure Report Card [1], while in 2022 water industry professionals cited the renewal and replacement of aging infrastructure as the water sector's most pressing challenge [2]. The prevalence of aging or outdated infrastructure in unprecedented contexts (e.g., climate change, population increases) leaves water systems especially vulnerable. For instance, in February 2021, a series of severe winter storms—commonly referred to collectively as Winter Storm Uri, the name we hereafter use [3]—crippled water infrastructure systems across Texas, causing extensive pipe and equipment failures and widespread service disruptions [4,5].

In the context of water infrastructure systems, resilience—"the ability to prepare and plan for, absorb, recover from, or more successfully adapt to actual or potential adverse events" [6]—can be impacted by numerous interacting factors. For instance, physical asset reliability, network structure, system design, management decisions, and customer demands all contribute to system performance during normal operations and extreme events like Winter Storm Uri [4,5]. Pipe failures, a common problem in U.S. water distribution systems, reflect a lack of physical asset reliability and can threaten both water supply and water quality [7]. On the other hand, network structure—meaning topology, or the way in which major system components such as water sources, pumping facilities, transmission mains, and pressure zones are spatially arranged and connected—determines how water moves through a system to ultimately provide adequate service to customers [8,9]. While these two components of water infrastructure resilience—pipe failures and network structure—are often analyzed individually, they are interrelated: network structure determines the impact of pipe failures on a system-wide scale [10,11]. As such, when assessing water infrastructure resilience, it is important to consider how these factors interact to impact overall system performance, as measured by the capacity to provide safe and reliable drinking water to customers.

Here, we present a system-wide assessment of water infrastructure resilience that considers performance with regard to pipe failures and network structure. We do so by comparing normal operating conditions

* Corresponding author.
E-mail address: linasela@utexas.edu (L. Sela).

https://doi.org/10.1016/j.ress.2023.109910
Received 30 April 2023; Received in revised form 21 November 2023; Accepted 23 December 2023
Available online 24 December 2023

(NOC) and emergency operating conditions (EOC), which can be precipitated by natural disasters or other severe system disruptions. Comparing these two operating scenarios is especially important because systems often behave in unprecedented or unexpected ways when acutely stressed, revealing or heightening vulnerabilities and dependencies between system components. Our framework evaluates how pipe failures and network structure interact to impact overall system performance and identifies targeted areas for improvements such as pipe rehabilitation and replacement projects. The results offer insights to utilities seeking to identify both asset and network vulnerabilities as they work to improve overall resilience to extreme events.

Given the importance of pipelines in overall water infrastructure system resilience, researchers have extensively studied and modeled pipe failures using various approaches [12]. Broadly, pipe failure research has sought to identify drivers and trends and predict pipe failures, with the overall goal of improving asset management to reduce costs, minimize service disruptions, and protect public health and safety (e.g., [13,14]). Descriptive analyses, which attempt to characterize pipe failure occurrence to reveal insights into spatial or temporal trends, have been conducted both as stand-alone studies (e.g., [15]) and as precursors to predictive models (e.g., [16]). For instance, researchers have applied spatial statistics and clustering approaches to identify spatial patterns (e.g., hot- and cold-spots) in pipe failures (e.g., [15–18]). Predictive models, on the other hand, use available historical data on past failures to anticipate future pipe failures. Such approaches have included physical, statistical, and data-driven models [12,19-23]. For a detailed review of the methods used in pipe failure prediction modeling, see [12,24]. While these analyses improve asset management practices by identifying patterns and helping utilities anticipate future repair needs, focusing on failure prediction and pipe condition assessment typically overlooks the system-wide impacts on performance and serviceability that result from pipe failures. Further, the long-term (typically multi-year) breadth of such studies can obscure rare but severe individual events which produce substantial, unanticipated numbers of pipe failures in a short period of time, impacting both system performance and recovery time.

At the same time, network structure is a critical factor which contributes to water infrastructure resilience. A separate, extensive body of work exists around modeling water infrastructure systems to simulate disruptions and identify network vulnerabilities. Researchers have examined water system resilience to extreme events through the development of methods such as global resilience analysis [8], graph-theoretic approaches [25], and fragility curves [9]. Examples of the types of extreme events that have been simulated and analyzed include seismic activity (e.g., [9,26-28]), intentional/malicious attacks (e.g., [29]), flood hazards (e.g., [28]), pipe failures (e.g., [30,31]), demand increases (e.g., [8,31]), and contamination events (e.g., [8]). Pipe failures have also been examined through the application of network indices such as betweenness centrality [11] and fractality [10], and in relation to variations in reliability and resilience over time as infrastructure deteriorates [32]. Broadly, modeling-based network resilience studies simulate a range of hypothetical disruptions or events occurring in abstracted networks of synthetic or real-world systems and combine hydraulic modeling with assessments of system vulnerability and recovery strategies. Studies in this arena often lack information about actual extreme events and system responses to disruptions, relying on simulated system behavior which might not be validated against measured performance. Modeling exercises provide valuable insights into potential system vulnerabilities in unknown contexts; however, abstractions make assumptions about system behavior during NOC and EOC and thus can have limited usability during an actual emergency.

Departing from literature, we identify three main gaps in the existing body of work. First, pipe failures and network structure are critical components of system performance, but these two factors are frequently assessed independently without consideration for how they interact to impact resilience during both NOC and EOC. Second, pipe failure analyses are long-term (multi-year) and typically do not considered the role of discrete extreme events, which can produce significant increases in failures with system-wide impacts in a short period of time. It is especially critical to examine rare—but high impact—events because such disruptions strain water systems and tend to occur when utility management resources are stressed in other ways. Finally, analyses considering network structure and resilience to extreme events often rely on abstractions of systems and simulated disruptions, potentially missing unexpected behaviors or responses that emerge during real events. While many utilities collect pipe failure records and operational data, such information is often not considered on shorter temporal scales (sub-annual) or related to overall system performance. At the same time, real-world system monitoring data has frequently been unavailable at the high resolutions needed for detailed network resilience analyses. These challenges surrounding temporal scales and data availability have thus hindered the exploration of cumulative system-wide impacts of pipe failures and network structure during EOC and NOC.

We address the above gaps by focusing on long- and short-term system performance, with long-term representing multi-year NOC and short-term focusing on a discrete EOC period caused by an extreme event. Specifically, we analyze pipe failure records spanning 2004–2021 and storage data from a recent weather disaster in a major southern U.S. city. Our research objectives are as follows: 1) identify outlier pipe failure events in the data; 2) compare and contrast failure rates and trends across the water system during NOC and EOC; 3) explore the contribution of pipe failures and network structure to system performance during EOC; and 4) identify the worst performing areas of the system to inform targeted infrastructure improvements.

2. Methods

Fig. 1 summarizes the objectives, methods, and temporal and spatial resolutions in each phase of the analysis, which is applied to a large, urban water infrastructure system in the southern U.S. Our analysis begins with a long-term, system-wide analysis of pipe failure data using control charts. This is followed by an assessment of failure rates at the pressure zone scale at both short- and long-term temporal scales. We then focus on a period of EOC to assess technical system performance and resilience, as measured by available stored water, and investigate the impact of pipe failures and network structure. Finally, we narrow the analysis to a single pressure zone and apply the density-based spatial clustering of applications with noise (DBSCAN) algorithm [33] to identify areas for targeted asset improvements and test NOC and EOC hotspot agreement.

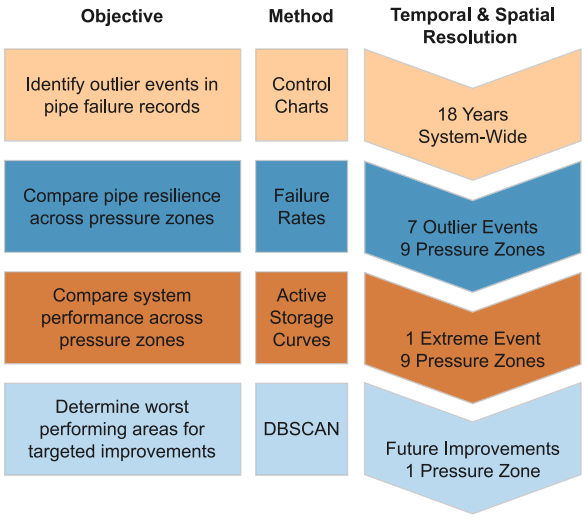

Fig. 1. Study approach including the objective, method, and temporal and spatial resolution for each phase of analysis.

2.1. Study area and data

The study area is a large southern U.S. city that experiences long, hot summers and short mild winters [34]. Section S1.1 in the Supplemental Materials (SM) describes the local environmental conditions (average temperature and precipitation) in the study area across the 18-year study period. One of the most historically significant weather events to impact the area occurred in February 2021 when Winter Storm Uri devasted much of the southern U.S. [3]. The area experienced snow, freezing rain, and multiple days of sub-freezing temperatures between February 10–20, 2021 [3], which in turn led to widespread electrical blackouts [35] and infrastructure failures across communication, healthcare, and water systems [36,37]. Winter Storm Uri caused historic levels of damage and impacts to communities; in Texas alone, 40 % of community water systems declared boil water notices [38], and approximately 49 % of residents lost access to running water for more than two days [39].

The study area is served by a municipal water and wastewater utility that is classified as "very large" by the U.S. EPA [40] and saw substantial impacts from Winter Storm Uri. The water distribution system is supplied by three water treatment facilities and consists of nine pressure zones and approximately 9334 km (5800 miles) of pipes. System-wide, the average daily water demand supplied is approximately 529,958 m^3 (140 millions gallons (MG)). Pressure zones are designated areas within which a consistent hydraulic grade line is maintained and are the primary spatial unit used by the utility for operations and management. Figure S2 in the SM shows the layout of the distribution system, including the three water treatment plants, nine pressure zones, and ground elevation ranges of the served areas in each pressure zone. The water utility provided the research team with approximately 18 years of pipe failure repair records from 2004 to 2021 which included the date of repair and pipe identification number; pipe failures refer to any leak, break, or rupture requiring a repair by the utility. GIS files of the water distribution system pipe network and pressure zone boundaries were also provided, allowing repairs to be geolocated in the pipe network, classified by pressure zone, and represented as point data. Hourly discharge and storage tank volumes were provided by pressure zone (in MG) for February 1, 2021–March 15, 2021, which included Winter Storm Uri. Given the significant disruptions cause by Winter Storm Uri, this time period (February 13–23, 2021) is considered in this study as an example of EOC.

2.2. Identifying extreme outlier events

To compare pipe failures during NOC and EOC, outlier events were first identified based on available data. Control charts are an appropriate tool for analyzing pipe failure occurrence over time as they are frequently used to monitor processes with inherent variation and identify outliers or changing trends [41,42]. This analysis offers a variation on control charts that can be replicated by utility managers interested in identifying changing trends in pipe failures (e.g., gradual increases) or acute events in which a large number of failures occur (e.g., isolated changes).

Here, we apply the Shewhart-type control chart with three-sigma control limits [41] to the pipe failure data to identify outlier events. To identify distinct, multi-day extreme events, data were aggregated to a weekly resolution, with each datapoint representing the number of pipe failures per week across the entire water system. The control chart was used to partition the dataset into two categories: failures occurring during NOC (i.e., under the upper control limit (UCL)) and failures occurring during outlier events (i.e., above the UCL), where $UCL = \mu + 3\sigma$, μ is the mean, and σ is the standard deviation of the failures. Because pipe failure occurrence varies seasonally in many regions [43], including in this study area, the data were split into summer and winter samples, with winter defined as November–February and summer defined as March–October based on typical seasonal patterns in the study area [34]. Separate summer and winter UCL values were calculated based on three-sigma control limits, and outlier events were defined as two or more consecutive data points above the seasonal UCL. See Section S1.2 in the SM for additional information about the control chart analysis procedure.

2.3. Spatial comparison of pipe failures

After partitioning the dataset into NOC and outlier events, we analyzed failure rates spatially to determine if pipe failures occur consistently across the system. The pipe failure data were first aggregated to the pressure zone scale to match the water storage data. For each pressure zone and dataset (NOC and outlier events) the annual failure rate (*FR*) was calculated as the number of pipe failures divided by the total length of pipes in that pressure zone, with units of failures/kilometer/year. Failure rates were also calculated for all pressure zones during the EOC period. To compare pipe failure rates with other measures of system performance on a common scale (see Section 2.4), a normalized pipe performance index (*PPI*) was calculated for each zone as:

$$PPI = 1 - \left(\frac{FR - FR_{\min}}{FR_{\max} - FR_{\min}} \right)$$

where $FR_{\max}$ and $FR_{\min}$ refer to the highest and lowest failure rates, respectively, among the nine pressure zones.

2.4. Analyzing system performance during EOC

To estimate the overall state of the water system during an acute disaster, we examine the realized system performance and recovery during the Winter Storm Uri EOC period using resilience curves and recovery scenarios based on system-wide mass balance calculations. We first use active storage to measure system performance during EOC and compare across pressure zones. Active storage is calculated as the total volume of water in all storage tanks in each pressure zone at an hourly resolution. Active storage is a holistic indicator that reflects changes in demands (e.g., increased consumption due to pipe failures), reductions in supply (e.g., failures at the source or pumping stations that supply to the storage tanks), and other failures throughout the distribution system (e.g., leaks and fire flow). In other words, active storage represents the system's capacity to absorb disruptions or shocks in both supply and demand. To compare system performance across different pressure zones, normalized active storage curves were constructed for each pressure zone and two resilience metrics adopted from literature were calculated. See Section S1.3 in the SM for the procedure for creating the storage curves.

We measure resilience using a resilience index (*RI*), a duration-based metric that represents the proportion of time during a disruption in which the system is performing above a specified critical threshold, defined here by the utility as one-third of total storage capacity [44,45]. The second metric, absorptive capacity index (*ACI*), is magnitude-based and indicates the severity of a disruption based on the area between target and actual performance [45,46]. Similar to *PPI*, *RI* and *ACI* are measured on a scale of 0–1, with 0 representing worst performance and 1 representing best performance.

To compute the resilience index (*RI*), we first evaluate the storage state indicator (I_t) to identify if the active storage (s_t) at time t is greater than the critical storage (s_c), where the value of I_t is equal to 1 if the storage is greater than the critical level and 0 otherwise, as follows:

$$I_t = \begin{cases} 1 & \text{if } s_t \geq s_c \\ 0 & \text{otherwise} \end{cases}$$

Then, the *RI* for each pressure zone is calculated as the fraction of time that active storage is greater than the critical storage (s_c):

$$RI = \frac{\sum_{t=1}^{T} I_t}{T}$$

where (T) is the duration of the event in hours.

To compute the absorptive capacity index (ACI), we first determine the total potential magnitude of disruption (D), which represents an active storage (s_t) of 0 for full event duration and equals the entire area under the target storage (s_a) curve over duration T:

$$D = s_a T$$

The actual magnitude of the disruption (M) is calculated by finding the difference between the potential magnitude (D) and the area under the active storage (s_t) curve over the duration T:

$$M = D - \sum_{t=1}^{T} \frac{s_t + s_{t+1}}{2} \Delta t$$

where (Δt) is the resolution of the data. Then, ACI is calculated for each pressure zone as a ratio of the actual magnitude (M) over potential magnitude (D) of the disruption, subtracted from 1:

$$ACI = 1 - \frac{M}{D}$$

To further assess how network structure and pipe failures impact system performance, we constructed and evaluated a mass balance model of the system under different scenarios. The network mass balance model was constructed based on the flows between sources and zones, discharge, and storage levels in each zone. For each Zone j at time t, the daily flow (Q) into that zone is calculated as:

$$Q_{jt} = S_{jt+1} - S_{jt} + D_{jt} + \sum_{i=1}^{m} Q_{it}$$

where S_{jt} and S_{jt+1} are the daily active storage in Zone j at t and $t + 1$, respectively; D_{jt} is the daily discharge in Zone j; Q_{it} is the daily flow from Zone j to Zone(s) i; and m is the number of Zone(s) i located directly downstream of Zone j. Here, discharge refers to all water leaving the distribution system in a pressure zone, which includes water consumed by customers and any water lost via pipe failures and other losses. The model is used to estimate the supply, discharge, storage, and flows between sources and zones under four scenarios: (A) NOC; (B) EOC, at the point when the system was most vulnerable (i.e., the peak of the disaster); (C) a recovery scenario that reflects the realized discharge in Zone 1 during EOC; and (D) a hypothetical recovery with reduced pipe failures, and therefore reduced discharge, in Zone 1. To discern the impact of reducing pipe failures in Zone 1 on the rest of the system, the two recovery scenarios (C and D) are modeled under the same simplified operating rules with only Zone 1 discharge changing.

2.5. Identifying hotspots for targeted asset management

After evaluating system performance, our next objective is to identify areas for targeted infrastructure improvements to increase resilience. However, pressure zone-scale measurements do not provide a fine enough resolution for utility managers to direct limited resources or investigate sub-pressure zone problem areas during NOC and EOC. Spatial analysis techniques enable us to identify areas within pressure zones with the highest concentrations of failures (i.e., "hotspots") and compare temporally [15,17]. Here, we use the DBSCAN algorithm [33,47] to identify clusters of pipe failures during NOC, focusing on the pressure zone with the highest pipe failure rate. We then compare NOC clustering results with pipe failures that occurred during EOC to determine how well the hotspots emerging during NOC align with, or predict, EOC failures. Practically, these results can assist utilities in targeting the worst performing areas and support decision making by indicating whether upgrading pipes in NOC hotspots will also improve performance during EOC.

The DBSCAN algorithm has two parameter inputs, ε (radial distance) and N_s (minimum number of points), which determine the expected density for cluster formation [33]. In our context, ε defines the radius of a neighborhood with respect to a point representing the location of a pipe failure, and N_s determines the number of points, i.e., additional pipe failures, that must exist within that radius to form a cluster. If the number of points within the specified radius ε is greater than N_s, the density is higher than expected, and a cluster, or hotspot, is formed. The decision maker's task then is to determine the appropriate ε and N_s for the context, ideally selecting values based on domain knowledge and keeping one parameter constant while varying the other [48]. Here, we apply an ε value of 300 m (~984 ft), which is approximately two average city blocks in the study area's downtown, an appropriate radius for targeted asset management improvements based on utility practice. With a set ε value of 300 m, we vary the N_s parameter to present a range of results. Finally, to quantify how well NOC clusters align with failures that occurred during EOC, we apply the principles of classification modeling to calculate precision (P) and recall (R) [49]. See Section S1.4 in the SM for additional information about the DBSCAN algorithm, parameter selection, and precision and recall calculations in this context.

3. Results

Here, we present the results of the four-step analysis approach. The control chart identified seven outlier events which were used to delineate the pipe failure data into NOC and outlier datasets. Failure rates were calculated for the nine pressure zones during NOC, all outlier events, and EOC (Winter Storm Uri) to assess spatial and temporal variation in pipe failure occurrence. To explore the influence of pipe failures and network structure on resilience during EOC, system performance is then quantified and compared spatially by pressure zone. Finally, we present a spatial clustering analysis of pipe failures in the zone with the worst PPI to examine hotspot agreement between NOC and EOC and identify areas for targeted asset management improvements.

3.1. Identifying extreme outlier events

Fig. 2 shows the control chart of pipe failure data across the approximately 18-year study period. For the summer dataset, $\mu = 7.15$, $\sigma = 5.37$, and $UCL = 23.27$ failures/week; for the winter dataset, $\mu = 11.73$, $\sigma = 9.13$, and $UCL = 39.12$ failures/week. As reflected in the mean, standard deviation, and UCL values, the data display a seasonal trend, with more pipe failures and greater variability occurring during winter, on average. Pipe failures typically peak in January or February and also increase during summer months in some years, though to a lesser extent than in winter (Fig. 2).

Using the control chart with seasonal UCLs, seven outlier events were identified, with four occurring in summer and three in winter (Fig. 2). Table 1 describes the seven events, including the start and end dates, total duration, and total number of pipe failures. Event 4 was the most prolonged and accounted for the greatest total number of breaks, with 248 failures occurring over 70 days. Event 7 was the most intense event in terms of failures per day, with 148 failures occurring over the course of 15 days. Notably, Event 4 corresponds to the region's drought of record, which reached its height in the summer of 2011 [50]. Event 7 corresponds to Winter Storm Uri, which devastated the region in February 2021 [3,36]. Both failure events significantly exceeded their seasonal UCLs (Fig. 2), showing that the control chart method is effective at identifying failure events caused by the most extreme weather, and can be seamlessly applied by other utilities to track various types of asset failures.

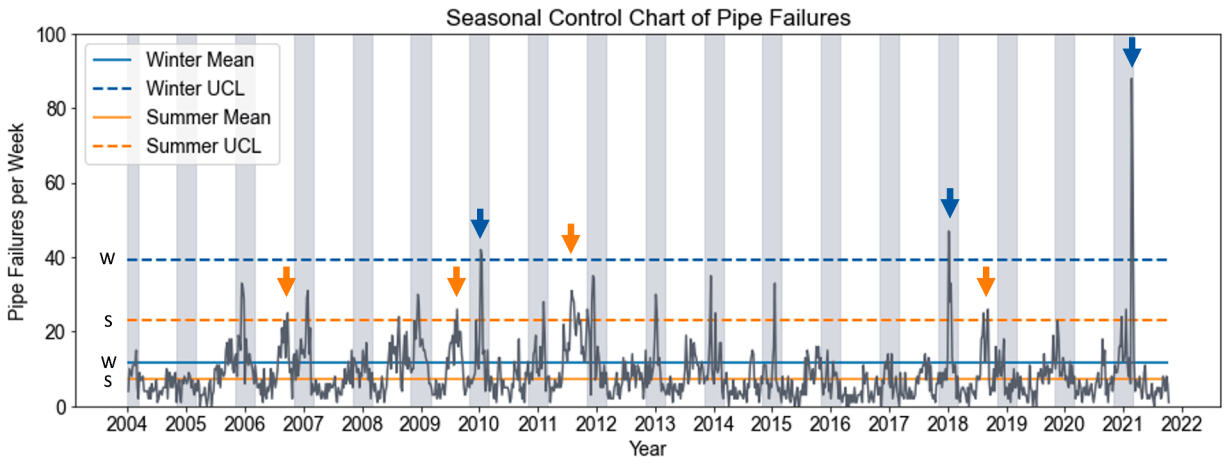

Fig. 2. Control chart of pipe failures showing seasonal UCLs and identified outlier events. The seasonal mean (solid) and UCL (dashed) are shown for summer (S, orange) and winter (W, blue). Arrows point to events in which the number of pipe failures exceeded the seasonal UCL (i.e., outlier events). Winter is defined as November–February and summer as March–October. Vertical shaded areas correspond to winter months. (For interpretation of the references to color in this figure legend, the reader is referred to the web version of this article.)

Table 1
Outlier events identified via control chart based on consecutive weeks above the UCL (Fig. 2).

Event #	Start date	End date	Duration (days)	Number of pipe failures
1	2006-08-13	2006-09-24	41	119
2	2009-07-26	2009-09-06	42	125
3	2010-01-03	2010-01-17	15	85
4*	2011-07-17	2011-09-25	70	248
5	2017-12-31	2018-01-21	22	108
6	2018-08-05	2018-09-09	34	99
7**	2021-02-14	2021-02-28	15	148

* Height of drought of record in study area.
** Winter Storm Uri.

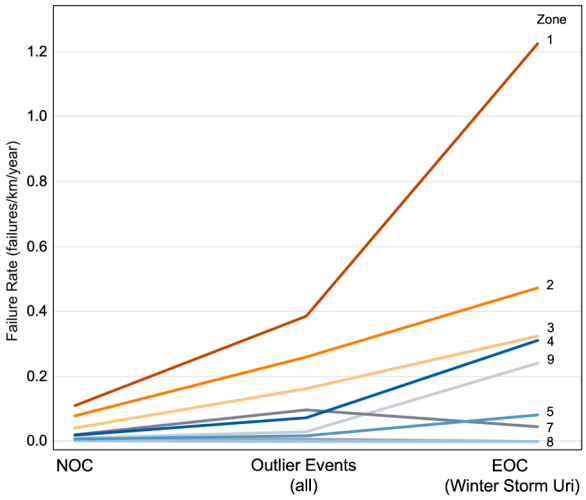

Fig. 3. Failure rates per pressure zone during NOC, outlier events, and EOC. Delineations for the three datasets are based on the control chart analysis (Fig. 2).

3.2. Spatial comparison of pipe failure rates

Based on the control chart results (Fig. 2), the full dataset of 8010 total failures was divided into three datasets: NOC (i.e., datapoints below the UCL; 7078 failures), all outlier events (i.e., the seven events above the UCL, 932 failures), and EOC (Winter Storm Uri, i.e., outlier Event 7; 148 failures). Notably, not all outlier failure events are extreme events or cause a utility to enter EOC; systems are generally robust enough to absorb a certain level of deviation from the norm. Of the seven identified events, we specifically investigate Winter Storm Uri as an example of EOC because utilities throughout the region were forced to operate under emergency protocols and the disaster inflicted historic impacts on infrastructure and communities [5]. Fig. 3 shows the failure rates, by pressure zone, for these three timeframes. During NOC, the failure rates for all pressure zones were below 0.2 failures/km/year, with Zones 1, 2, and 3 having the highest failure rates and Zones 4–9 having failure rates of 0.02 failures/km/year or less. During the seven identified outlier events, failure rates increased for all zones except 6 and 8 when compared to NOC. During EOC, failure rates for Zones 1, 2, 3, 4, 5, and 9 increased when compared to the full outlier dataset, while failure rates for Zones 6, 7, and 8 were the same or lower. For all three timeframes, Zones 1, 2, and 3 had the highest failure rates, with Zone 1 consistently highest. Zone 1 also experienced the greatest failure rate increase during EOC compared to NOC and the full set of outlier events (increases of 1.12 and 0.84 failures/km/year, respectively).

Examining failure rates across all pressure zones over the three specified timeframes reveals spatial variability between zones in terms of the reliability of pipe assets, as the nine pressure zones do not perform equally (Fig. 3). While the magnitude of failure rates varied significantly between NOC and EOC, the ranking from worst (highest failure rates) to best (lowest failure rates) remained largely the same, especially for the three worst performing zones (1, 2 and 3). This consistency across different operating contexts shows that vulnerabilities present during NOC (i.e., susceptibility to pipe failures) are exacerbated during EOC.

While Zones 1, 2, and 3 consistently performed worst in terms of failure rates, failure rates alone do not measure actual system performance (i.e., available water to be delivered to customers and continuation of service). Though it is expected that the zones with the worst failure rates would also exhibit the worst system performance due to greater water loss via pipe failures, this assumption can only be tested in a severe emergency. Generally, when pipe failures occur a water infrastructure system is robust enough to continue providing service to customers without disruption. However, Winter Storm Uri was such a

severe disaster that serviceability was substantially compromised, as indicated by a system-wide boil water notice, extensive depletion of water storage, and water outages in large portions of the distribution system. This acute disaster provides an opportunity to understand how spatial variations in pipe failure rates contributed to performance across the system.

3.3. Analyzing system performance during EOC

To examine whether zones with the highest pipe failure rates perform worst, we examine the performance of each pressure zone during EOC. Fig. 4 shows normalized active storage curves—based on hourly storage measurements—for all nine pressures zones. During the EOC period from February 13–23, 2021 (total duration *T* of 240 h), all zones exhibited a substantial decrease in performance beyond typical daily variability. Zones 1 and 3 showed the first signs of abnormal behavior, with performance dipping below average mid-day on February 13 and failing to recover. Zones 2, 4, 7, and 9 followed, similarly dropping below average on February 15 (Zone 9 briefly recovered on February 16 before dropping again). Zones 5, 6, and 8 followed on February 16. All zones remained below their average performance for at least 5 days.

Fig. 5 compares the pipe performance index (*PPI*) (calculated based on EOC failure rates, Fig. 3) with two active storage curve metrics—absorptive capacity index (*ACI*) and resilience index (*RI*)—for each pressure zone. The results show a notable discrepancy between pipe performance and system performance during EOC. In terms of absorptive capacity, Zones 4 and 1 performed best, with *ACI* scores of 0.73 and 0.71, respectively. Zones 7 and 9 performed worst, each with *ACI* scores of 0.43, followed by Zones 8 (0.46), 6 (0.49), 5 (0.51), 3 (0.57), and 2 (0.63). In terms of resilience, Zones 4 and 1 again performed ahead of all other zones, with *RI* scores of 0.81 and 0.80, respectively. Zone 6 performed worst, with an *RI* score of 0.36, followed by Zones 9 (0.45), 8 (0.48), 7 (0.50), 5 (0.54), 2 (0.55), and 3 (0.61). Comparing these three indices for each zone reveals that pipe failures did not correspond to actual system performance during EOC. For instance, Zones 5–9 had the highest *PPI* but the worst *ACI* and *RI*, while Zone 1 had the worst *PPI* by far but ranked second best in *ACI* and *RI*. Zones 2 and 4 were the most consistent across the three metrics, followed by Zone 3.

One potential explanation for this discrepancy between the pipe performance index and the active storage curve metrics lies in the network structure, as revealed through calculating changes in supply, discharge, and storage in the system. Fig. 6 shows the network layout and mass balance of supply, discharge, storage, and flows across the system during both NOC (Fig. 6(A)) and EOC (Fig. 6(B)). The active storage in each pressure zone is shown, with the discharge arrows indicating the performance level: green/solid = healthy performance, storage above critical threshold and discharge equal to or exceeding NOC levels; yellow/dotted = poor performance, storage at or below critical threshold and only partial NOC discharge met; red/dashed = very poor, storage below critical threshold and no water discharged. During NOC, the water treatment plants have a capacity of approximately 529,957 m^3/day (140 MGD), with total discharge equaling approximately 465,605 m^3/day (123 MGD) (Fig. 6(A)). Water is pumped from the treatment plants directly to Zones 1–4 and then pumped out to Zones 5–9. Located in the core of the system, Zone 1 has the highest level of connectivity to the sources and other zones with a degree centrality of 4 [51] and receives the most water from the treatment plants (166,558 m^3/day, 44 MGD), while also pumping the most water to other zones (68,137 m^3/day, 18 MGD). Conversely, Zones 5–9 have only one connection each and rely entirely on water pumped through other zones.

Fig. 6(B) shows a system-wide snapshot from February 17–18, 2021, when performance was worst (Fig. 4). Zones 1, 2, and 4 maintained low levels of storage and were able to maintain partial discharge (categorized as "poor" performance), while Zones 5–9 had fully depleted storage, with no water discharged (categorized as "very poor" performance). Notably, during this time discharge in Zone 1 was 273 % *greater* than NOC discharge levels. With a substantially higher pipe failure rate than all other zones during this EOC period (Fig. 3), this excess consumption was primarily due to extensive pipe failures occurring throughout the zone. Due to the network structure, even with increased supply (the utility increased treatment capacity to 643,520 m^3/day, 170 MGD), this extra supply was largely being discharged into Zone 1 and not reaching Zones 5–9. In other words, the water that should have been pumped from Zones 1–4 into Zones 5–9 was instead consumed in Zone 1, much of it through water loss via broken pipes. As the negative impacts of pipe failures in Zone 1 cascaded outward, Zones 2–4 continued to receive partial supply due to their connection to the three water sources (Fig. 6(B)), leading to less severe overall impacts on performance, as reflected in their high *ACI* and *RI* scores (Fig. 5). Zones 5–9, which had high *PPI* scores due to very few pipe failures, experienced the worst performance with low *ACI* and *RI* scores (Fig. 5) due to the lack of available water moving into these zones (Fig. 6(B)).

To better investigate how the network structure allowed the high failure rate in Zone 1 to impact performance across the system, we evaluated two recovery scenarios from the EOC point shown in Fig. 6(B). Fig. 6(C) and (D) show how reducing the pipe failures in Zone 1, and therefore reducing excess discharge, improves overall system recovery. In Scenario C (Fig. 6(C)), representing the realized Zone 1 discharge during the storm, Zone 1 discharge remains high: all of the 264,979 m^3/day (70 MGD) available to Zone 1 is consumed by that zone (a 253 % increase from NOC discharge levels), and no water remains to be pumped to other zones. Only Zones 1–3 have storage above the critical threshold and meet NOC discharge levels, Zones 4 and 7 have storage above the critical threshold but only meet partial NOC discharge, and Zones 5, 6, 7, and 9 have depleted storage and no water discharged. In hypothetical recovery Scenario D, Zone 1 discharge remains elevated, but the excess consumption due to pipe failures is reduced by approximately 50 %: only 189,270 m^3 (50 MGD) of the available 264,979 m^3/day (70 MGD) is consumed in Zone 1 (a 192 % increase from NOC), leaving 17 MGD available to be pumped to other zones. As a result, Zones 7–9 are able to meet 100 % of NOC discharge levels while maintaining storage above the critical threshold, Zone 5 storage is above the critical threshold and partial NOC discharge levels are met, and only Zone 6 remains in "very poor" status. The result is a more equitable allocation of water across zones and more distributed, system-wide recovery, with only 1/9 pressure zones performing at "very poor" in Scenario D, compared to 4/9 zones in Scenario C. Overall, the performance metrics and network mass balance model indicate that improving the reliability of pipes in Zone 1 to reduce failures has system-wide benefits by preventing detrimental impacts from cascading downstream and improving recovery when supply to the external zones is disrupted.

3.4. Identifying hotspots for targeted asset management

With pipe failures in Zone 1 having a significant impact on performance throughout the entire system, the next objective is to determine which areas in this zone warrant infrastructure investments. Given its size (approximately 1800 km of pipeline over 240 km^2), targeting the entire pressure zone for pipe improvements is not logistically or financially feasible. It is also important to understand prior to investing in a given area if the locations that perform poorly during NOC align with high failure areas during EOC. With most utilities having limited resources to repair or replace waterlines, spatial analysis using DBSCAN offers a solution for assessing this agreement and pinpointing locations for targeted asset management strategies.

Here, we conduct a spatial analysis within Zone 1 to identify high density pipe failure areas and test whether NOC failures predict EOC failures. Fig. 7 shows the resulting clusters (shaded areas) from four DBSCAN analysis runs using the 18-year pipe failure dataset (excluding

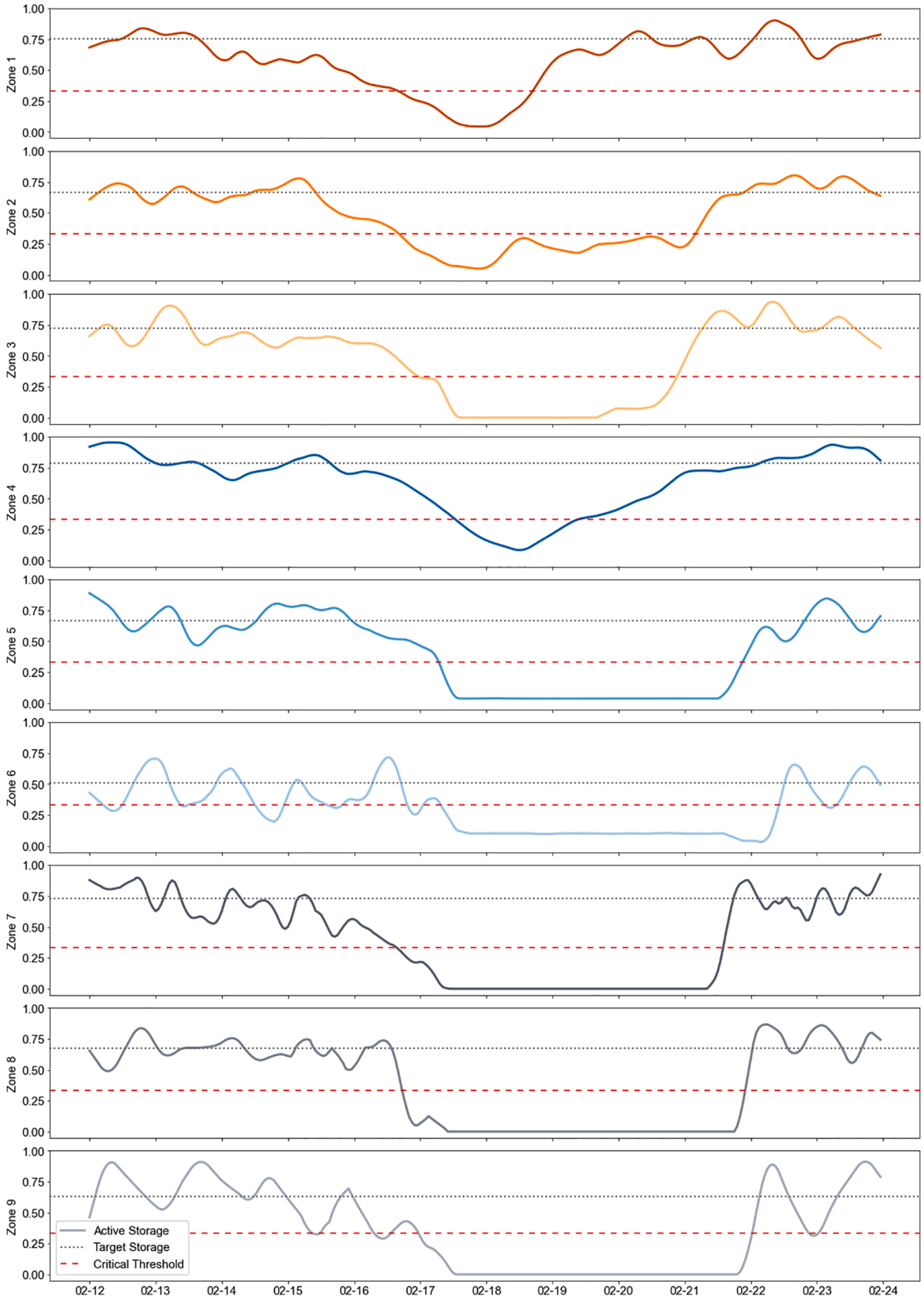

Fig. 4. EOC normalized active storage curves for the nine pressure zones from February 12–24, 2021, with 1 representing the normalized storage capacity. Solid lines indicate active storage (s_t); dotted and dashed lines show target storage (s_a) and the critical threshold (s_c), respectively.

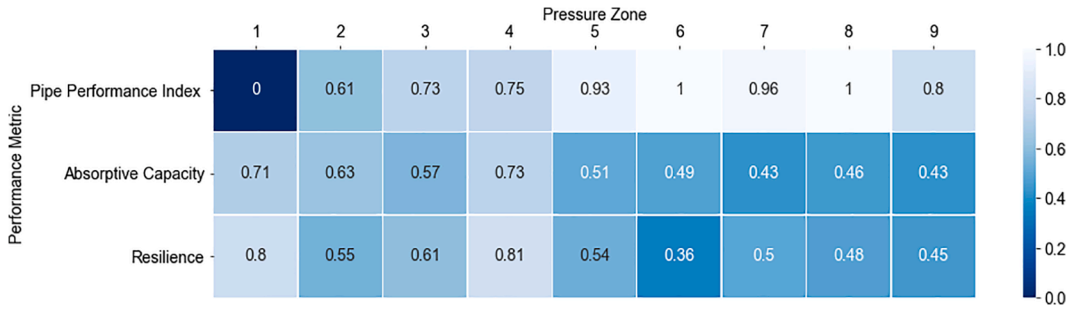

Fig. 5. Heatmap comparing three performance indices across nine pressure zones during EOC: pipe performance index (*PPI*), absorptive capacity index (*ACI*), and resilience index (*RI*). For all indices, 0 (dark blue) indicates worst performance, and 1 (light blue) indicates best performance. (For interpretation of the references to color in this figure legend, the reader is referred to the web version of this article.)

EOC failures) where ε= 300 m and N_s is varied at 6, 10, 13 and 21. N_s values were selected based on the distribution of the number of pipe failures across the entire zone (see Section S1.4 in the SM for the parameter selection process). Pipe failures that occurred during EOC (red circles) are overlaid on top of the clusters, showing the level of agreement between NOC cluster formation and EOC failures for each run. Table 2 provides summary statistics for each analysis run (A) in addition to the classification results (B) which quantify how well the clustering algorithm captured, or predicted, EOC failures.

While the four runs result in clusters of different shapes and sizes, a quick visual inspection of Fig. 7 shows the clustering algorithm (based on NOC failures) was largely successful at capturing EOC failures. As expected, loosening the constraints around cluster formation by decreasing the number of points required (N_s) results in more total clusters and larger average cluster size, whereas tightening constraints with a higher N_s value results in fewer total clusters and smaller average cluster size (Table 2). With a lower number of required points, more of the EOC failures fall within established clusters, and this amount decreases as N_s is increased (Fig. 7). There is also general agreement between the four runs that a hotspot of pipe failures exists in the center/northeast quadrant of the map area. In other words, there is an area in this pressure zone that is consistently identified, across all runs, as a problem area based on significantly higher densities of pipe failures. While utility managers might vary the exact scope of their work (e.g., total area targeted for repairs and replacement) based on available funds and other logistical factors, these results indicate that this area would be a reasonable place to begin planning for infrastructure improvements.

Precision and recall were used to quantify the agreement between clusters and EOC failures and evaluate the algorithm's performance at each value of N_s (Table 2). Fig. 8 plots the precision and recall curve over the four runs, showing a clear bend at $N_s = 13$, where $P = 0.7$ and $R = 0.8$. From a classification modeling perspective, a N_s value around 13 is therefore the optimal choice for capturing the most EOC failures without creating an unnecessary number of clusters that are larger in size (i.e., overfitting the model). Overall, the results show strong hotspot agreement between NOC and EOC. In addition, this analysis offers a demonstration of a flexible application of the DBSCAN algorithm that can be recreated by utilities for asset management and fine-tuned based on the needs and constraints of the utility.

4. Discussion

Our results have several implications for how utilities consider system behavior and planning for extreme events. Below, we outline how these insights might be generalized to other utilities and sectors seeking to improve resilience.

4.1. Comanaging stressed water and utility resources

The cooccurrence of outlier failure events with natural disasters, as revealed in the control chart and failure rates (Figs. 2 and 3), highlights the need to examine system behavior during these events more extensively. During extreme events, utility resources are already heavily stressed in a number of ways. For instance, during the drought of record (Table 1, Event 4), utilities were attempting to conserve water and most of the region was under water use restrictions [52–54]. A significant increase in pipe failures meant additional water loss (via breaks and leaks) at a time when water resources were extremely limited. Similarly, during the Winter Storm Uri emergency (Table 1, Event 7), utility resources across the region were stressed as crews contended with power outages, poor road conditions, and increased water demands due to private side leaks and customer usage [4,5]. Understanding that these outlier pipe failure events can occur during disasters when water infrastructure systems are simultaneously stressed in other ways points to the need for further investigation to increase resilience when systems are pushed beyond NOC.

4.2. The case for holistic analysis of pipe and system failures

Overall, our analysis of pipe and system performance using *PPI*, *ACI*, *RI*, and network mass balance empirically shows that zones with the worst performance in terms of pipe failures do not necessarily experience the worst system performance during an emergency event. Rather, these results support an alternate conclusion that pipe failures impacted performance system-wide, and the effects were not localized or contained to individual zones. Though other factors can impact performance, in this disaster the network structure of the overall system allowed impacts to cascade from the zones with the worst *PPI* to the zones that were most vulnerable in terms of network connectivity. As a result, zones with the fewest pipe failures—which happened to be furthest from sources and reliant on single inputs—ultimately experienced the worst system performance. Importantly, this understanding of system behavior would have been overlooked had pipe failures and network structure not been considered holistically with system performance. These results indicate that investments made to improve pipe failure rates in the highest failing areas (e.g., through asset management repair or replacement efforts) could have system-wide benefits, depending on a system's structure and vulnerabilities.

4.3. Extreme event preparation informed by past failures

This work sought to assess the agreement between performance issues in NOC and EOC and determine how past failures could improve preparation for future events. In practical terms, the results of the spatial analysis show overall that most EOC failures occurred in areas that were already hotspots for pipe failures during NOC (Fig. 7). Therefore, targeting clusters identified by the DBSCAN algorithm should also improve asset performance during future extreme events. While this agreement may be expected, it offers utility managers concrete evidence that asset management improvements targeting NOC hotspots of poor pipe failures

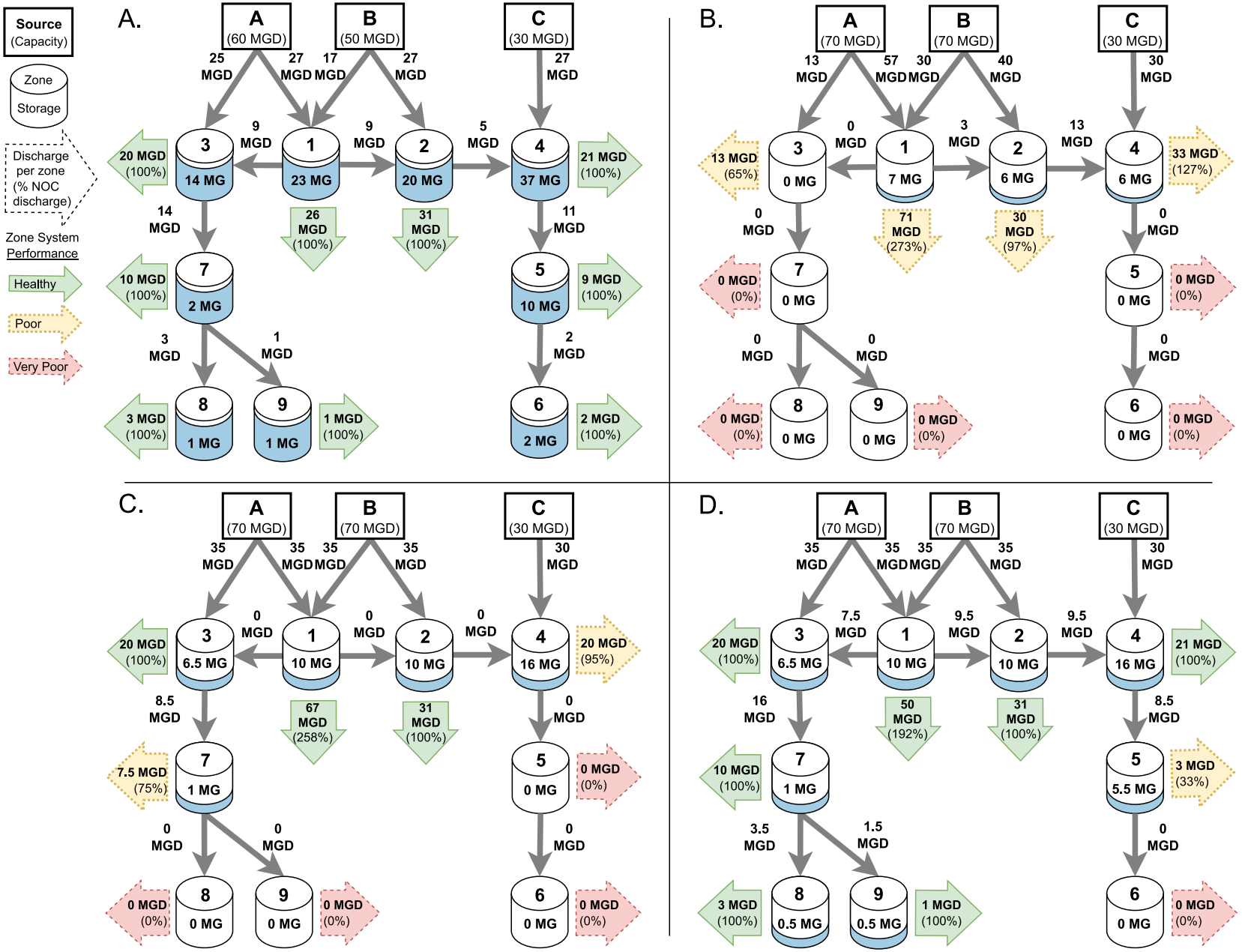

Fig. 6. System mass balance model showing water supply, storage and discharge in each zone, and flows between zones in: (A) NOC, (B) EOC—worst performance, (C) EOC—recovery under realized discharge, and (D) EOC—hypothetical recovery with reduced pipe failures in Zone 1. The gray arrows indicate daily flows, tank storage indicates active storage per zone, and discharge arrows indicate performance in each zone: green/solid = healthy performance, yellow/dotted = poor performance, red/dashed = very poor. (For interpretation of the references to color in this figure legend, the reader is referred to the web version of this article.)

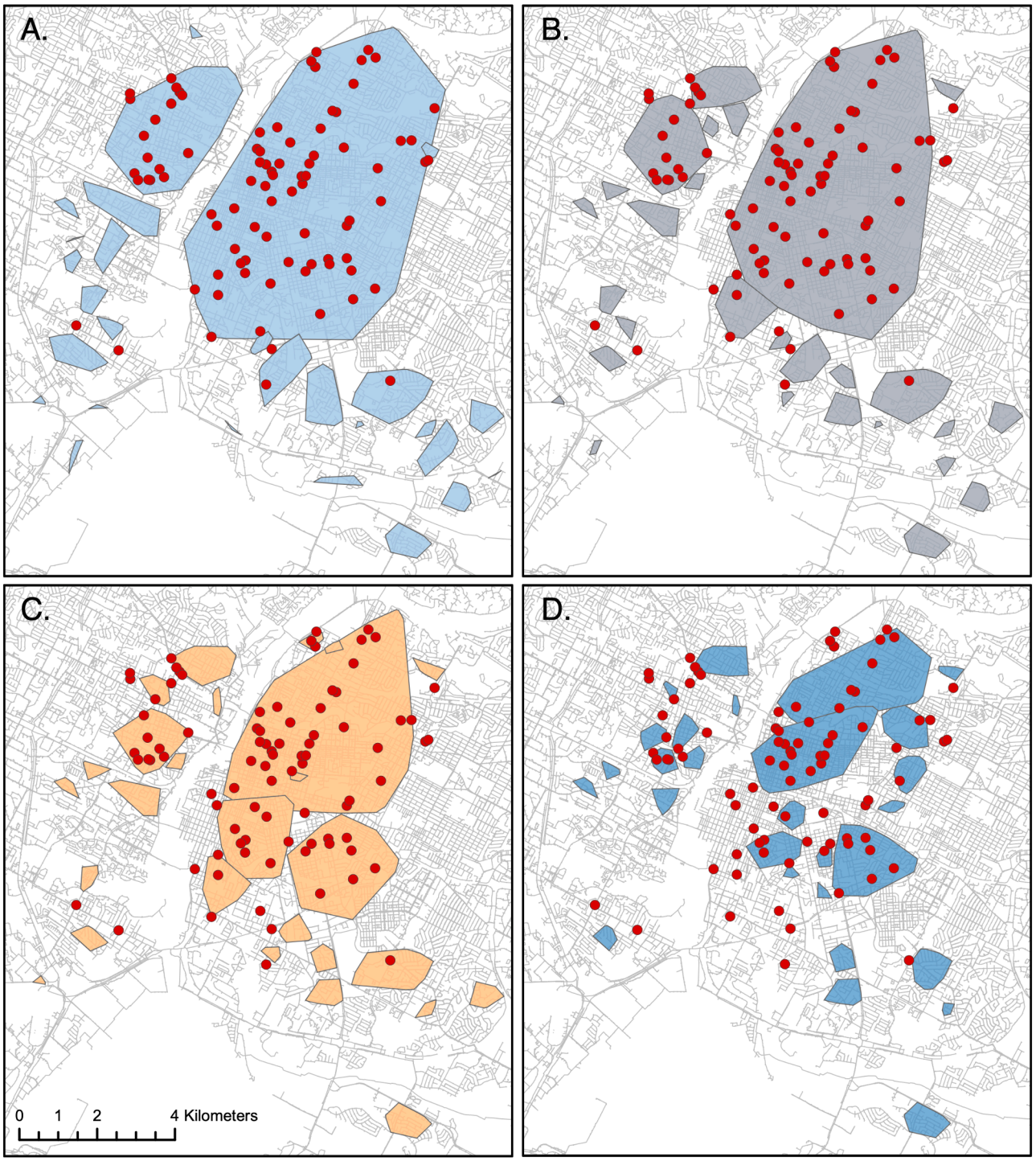

Fig. 7. DBSCAN results for a portion of Zone 1 overlaid with pipe failures that occurred during EOC, as indicated by red circles. For all runs, $\varepsilon = 300$ m. The minimum points required (N_s) within distance ε is equal to 6 (A), 10 (B), 13 (C), and 21 (D).

have the potential to bring system-wide benefits. However, these types of improvements are largely reactive, meaning the utility is responding to infrastructure that is already failing or underperforming. Utilities seeking to improve overall resilience might also consider changes to network structure (e.g., transmission between sources and zones) and facility siting (e.g., storage tanks) which can help to address network vulnerabilities. Such interventions are proactive investments which seek to improve systems overall or prevent failures from occurring in the first place. Inherent to the challenge of upgrading aging infrastructure and implementing capital improvement projects to increase resilience are the financial constraints facing most water utilities [2]. Notably, proactive infrastructure investments are costly and sometimes garner less organizational and public support because they lack the urgency and visibility of problems requiring reactive interventions (e.g., main breaks, equipment failures). While proactive projects can be difficult to implement due to lack of funds and the prevalence of more pressing problems, they are critical for building long-term system resilience.

Table 2
Clustering results for Zone 1 showing (A) summary statistics for DSCAN with $\varepsilon = 300$ m, and (B) EOC pipe failure classification results.

Percentile (failures per 300 × 300 m cell)	75th	90th	95th	99th
Expected failures (N_s)	6	10	13	21
A. Clustering results				
Number of clusters	55	47	41	29
Percentage of noise points	8 %	15 %	13 %	21 %
Cluster size (km^2):				
Maximum	36.4	29.6	17.6	5.8
Mean	1.2	1.0	1.0	0.8
Standard deviation	5.3	4.4	2.9	1.3
Pipe failures per cluster:				
Maximum	1943	1733	1125	485
Mean	64.5	69.5	73.9	80.3
Standard deviation	261.4	247.9	117.1	104.8
B. EOC classification results				
EOC failures per cluster:				
Maximum	67	59	35	17
Mean	2.2	2.1	2.1	1.7
Standard deviation	10.8	9.8	6.2	3.5
Total EOC pipe failures captured by clusters *(true positive)*	86	77	74	48
EOC pipe failures not captured by clusters *(false negative)*	6	15	18	44
Clusters not containing any EOC pipe failures *(false positive)*	50	43	31	16
Precision (*P*)	0.63	0.64	0.70	0.75
Recall (*R*)	0.93	0.84	0.80	0.52

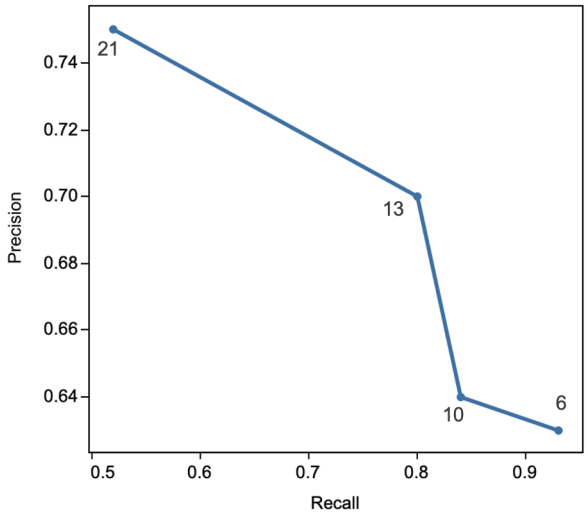

Fig. 8. Precision and recall results for DBSCAN analysis where $\varepsilon = 300$ m. Labels indicate N_s value (minimum points required within distance ε for cluster formation).

4.4. Data adequacy for assessing and improving resilience

Water distribution networks are complex systems whose performance may be impacted by a variety of factors, particularly during an emergency. Our analysis utilized pipe repair records, available stored water measurements, and discharge volumes to relate pipe failure rates and network structure to system performance during Winter Storm Uri. However, it must be acknowledged that other factors might have contributed to the depletion of water storage observed throughout the event. For instance, across the entire region, water utilities' ability to continuously meet demands was impacted by plumbing failures in homes and businesses, increased customer water usage (e.g., dripping faucets, storing water), and power outages at treatment and pumping facilities [4,5]. Identifying specific factors, such as private or public systems and human behavior, that contributed to lost reservoir storage is challenging due to the lack of available data and the simultaneous occurrence of multiple incidents during a chaotic emergency period. As such, we assume that impacts from these additional factors on storage were distributed evenly across the entire system and did not affect individual pressure zones more than others. Observed disparities in system performance between pressure zones are, therefore, attributed largely to known differences (i.e., pipe failures and network connectivity).

This analysis highlights the importance of having reliable data during emergencies, and additional data such as high-resolution demands and pressure sensor readings could provide an even more nuanced understanding of system behavior during extreme events. While the data employed here do not provide a complete picture of system behavior during an emergency, they still offer valuable insights into the ways in which physical asset failures and system design impact system performance. Finally, this work was enabled by a close partnership between the research team and utility, who provided data, guidance, and support throughout the study. This work highlights the mutual benefits of such collaborations and shows the value of establishing rigorous data collection and management practices, which support these types of system-wide analyses.

5. Conclusions

This study evaluated the role of pipe failures and network structure on system resilience. Most interestingly, our analysis revealed that pipe failures did not correspond to system performance on a pressure zone scale. Rather, the high-level network structure appears to have allowed negative impacts of pipe failures in the central zones to cascade to the outer portions of system. This study also confirmed a spatial agreement between failures that occurred in NOC and EOC. Using data that is commonly available at many municipal utilities (pipe failure records and storage tank levels), this approach may be adopted by other utilities wishing to evaluate system vulnerabilities and build long-term system resilience. Future analyses would benefit from additional sources of high-resolution data capable of capturing system behavior during an emergency, such as Advanced Metering Infrastructure and distributed pressure sensors. Additional studies should also work to better evaluate the role of human behavior and public perceptions on system performance by considering customer communication with utilities during emergencies and trends in reporting (e.g., 3-1-1 calls and service requests). Continuing to explore system behavior during extreme events is critical for building water system resilience to future disasters and the infrastructure challenges of the 21st century.

CRediT authorship contribution statement

Helena R. Tiedmann: Conceptualization, Data curation, Formal analysis, Writing – original draft, Writing – review & editing. **Kasey M. Faust:** Conceptualization, Writing – review & editing, Supervision, Funding acquisition. **Lina Sela:** Writing – review & editing, Supervision, Methodology, Funding acquisition, Conceptualization.

Declaration of competing interest

The authors declare that they have no known competing financial interests or personal relationships that could have appeared to influence the work reported in this paper.

Data availability

The authors do not have permission to share data.

Acknowledgments

The authors thank Austin Water for their guidance and support throughout this study. This work was supported in part by the National Science Foundation under Grants 1943428 and 2129801. Any opinions, findings, and conclusions or recommendations expressed in this material are those of the authors and do not necessarily reflect the views of the National Science Foundation.

Supplementary materials

Supplementary material associated with this article can be found, in the online version, at doi:10.1016/j.ress.2023.109910.

References

[1] American Society of Civil Engineers, "ASCE's 2021 American infrastructure report card | GPA: C-", ASCE's 2021 Infrastructure Report Card|. Accessed: Jan. 29, 2023. [Online]. Available: https://infrastructurereportcard.org/.
[2] American Water Works Association, "State of the water industry: executive summary", 2022. [Online]. Available: https://www.awwa.org/Professional-Development/Utility-Managers/State-of-the-Water-Industry.
[3] National Weather Service, "Valentine's week winter outbreak 2021: snow, ice, & record cold", National Weather Service. Accessed: Sep. 23, 2022. [Online]. Available: https://www.weather.gov/hgx/2021ValentineStorm.
[4] Glazer YR, et al. Winter storm Uri: a test of Texas' water infrastructure and water resource resilience to extreme winter weather events. J Extreme Events 2021: 2150022. https://doi.org/10.1142/S2345737621500226.
[5] Tiedmann HR, Spearing LA, Castellanos S, Stephens KK, Sela L, Faust KM. Tracking the post-disaster evolution of water infrastructure resilience: a study of the 2021 Texas winter storm. Sustain Cities Soc 2023:104417. https://doi.org/10.1016/j.scs.2023.104417.
[6] National Research Council. Disaster resilience: a national imperative. Washington, D.C.: The National Academies Press; 2012. https://doi.org/10.17226/13457.
[7] Folkman S. Water main break rates in the USA and Canada: a comprehensive study. Utah State University Buried Structures Laboratory; 2018.
[8] Diao K, Sweetapple C, Farmani R, Fu G, Ward S, Butler D. Global resilience analysis of water distribution systems. Water Res 2016;106:383–93. https://doi.org/10.1016/j.watres.2016.10.011.
[9] Klise KA, Bynum M, Moriarty D, Murray R. A software framework for assessing the resilience of drinking water systems to disasters with an example earthquake case study. Environ Model Softw 2017;95:420–31. https://doi.org/10.1016/j.envsoft.2017.06.022.
[10] Giudicianni C, Di Nardo A, Greco R, Scala A. A community-structure-based method for estimating the fractal dimension, and its application to water networks for the assessment of vulnerability to disasters. Water Resour Manag 2021;35(4): 1197–210. https://doi.org/10.1007/s11269-021-02773-y.
[11] Agathokleous A, Christodoulou C, Christodoulou SE. Topological robustness and vulnerability assessment of water distribution networks. Water Resour Manag 2017;31(12):4007–21. https://doi.org/10.1007/s11269-017-1721-7.
[12] Barton NA, Hallett SH, Jude SR, Tran TH. An evolution of statistical pipe failure models for drinking water networks: a targeted review. Water Supply 2022;22(4): 3784–813. https://doi.org/10.2166/ws.2022.019.
[13] Rifaai TM, Abokifa AA, Sela L. Integrated approach for pipe failure prediction and condition scoring in water infrastructure systems. Reliab Eng Syst Saf 2022;220: 108271. https://doi.org/10.1016/j.ress.2021.108271.
[14] Fan X, Zhang X, Yu XB. Uncertainty quantification of a deep learning model for failure rate prediction of water distribution networks. Reliab Eng Syst Saf 2023; 236:109088. https://doi.org/10.1016/j.ress.2023.109088.
[15] de Oliveira D, Garrett JH, Soibelman L. A density-based spatial clustering approach for defining local indicators of drinking water distribution pipe breakage. Adv Eng Inform 2011;25(2):380–9. https://doi.org/10.1016/j.aei.2010.09.001.
[16] Abokifa AA, Sela L. Spatiotemporal scan statistics for the identification of density-based clusters of pipe failure events in drinking water distribution systems. Computing in civil engineering 2019. Atlanta, Georgia: American Society of Civil Engineers; 2019. p. 306–13. https://doi.org/10.1061/9780784482445.039.
[17] de Oliveira D, Garrett Jr JH, Soibelman L. Spatial clustering analysis of water main break events. Computing in civil engineering (2009). Austin, Texas, United States: American Society of Civil Engineers; 2009. p. 338–47. https://doi.org/10.1061/41052(346)34.
[18] de Oliveira D, Neill DB, Garrett JH, Soibelman L. Detection of patterns in water distribution pipe breakage using spatial scan statistics for point events in a physical network. J Comput Civ Eng 2011;25(1):21–30. https://doi.org/10.1061/(ASCE)CP.1943-5487.0000079.
[19] Kleiner Y, Rajani B. Comprehensive review of structural deterioration of water mains: statistical models. Urban Water 2001;3(3):131–50. https://doi.org/10.1016/S1462-0758(01)00033-4.
[20] Nishiyama M, Filion Y. Review of statistical water main break prediction models. Can J Civ Eng 2013;40(10):972–9. https://doi.org/10.1139/cjce-2012-0424.
[21] St. Clair AM, Sinha S. State-of-the-technology review on water pipe condition, deterioration and failure rate prediction models! Urban Water J 2012;9(2):85–112. https://doi.org/10.1080/1573062X.2011.644566.
[22] Wilson D, Filion Y, Moore I. State-of-the-art review of water pipe failure prediction models and applicability to large-diameter mains. Urban Water J 2017;14(2): 173–84. https://doi.org/10.1080/1573062X.2015.1080848.
[23] Fan X, Wang X, Zhang X, ASCE Xiong (Bill) Yu PEF. Machine learning based water pipe failure prediction: the effects of engineering, geology, climate and socio-economic factors. Reliab Eng Syst Saf 2022;219:108185. https://doi.org/10.1016/j.ress.2021.108185.
[24] Dawood T, Elwakil E, Novoa HM, Gárate Delgado JF. Water pipe failure prediction and risk models: state-of-the-art review. Can J Civ Eng 2020;47(10):1117–27. https://doi.org/10.1139/cjce-2019-0481.
[25] Herrera M, Abraham E, Stoianov I. A graph-theoretic framework for assessing the resilience of sectorised water distribution networks. Water Resour Manag 2016;30 (5):1685–99. https://doi.org/10.1007/s11269-016-1245-6.
[26] Emamjomeh H, Ahmady Jazany R, Kayhani H, Hajirasouliha I, Bazargan-Lari MR. Reliability of water distribution networks subjected to seismic hazard: application of an improved entropy function. Reliab Eng Syst Saf 2020;197:106828. https://doi.org/10.1016/j.ress.2020.106828.
[27] Laucelli D, Giustolisi O. Vulnerability assessment of water distribution networks under seismic actions. J Water Resour Plan Manag 2015;141(6):04014082. https://doi.org/10.1061/(ASCE)WR.1943-5452.0000478.
[28] Yu J-Z, Whitman M, Kermanshah A, Baroud H. A hierarchical Bayesian approach for assessing infrastructure networks serviceability under uncertainty: a case study of water distribution systems. Reliab Eng Syst Saf 2021;215:107735. https://doi.org/10.1016/j.ress.2021.107735.
[29] Wu Y, Chen Z, Gong H, Feng Q, Chen Y, Tang H. Defender–attacker–operator: tri-level game-theoretic interdiction analysis of urban water distribution networks. Reliab Eng Syst Saf 2021;214:107703. https://doi.org/10.1016/j.ress.2021.107703.
[30] Berardi L, Ugarelli R, Røstum J, Giustolisi O. Assessing mechanical vulnerability in water distribution networks under multiple failures. Water Resour Res 2014;50(3): 2586–99. https://doi.org/10.1002/2013WR014770.
[31] Chu-Ketterer L-J, Murray R, Hassett P, Kogan J, Klise K, Haxton T. Performance and resilience analysis of a New York drinking water system to localized and system-wide emergencies. J Water Resour Plan Manag 2023;149(1):05022015. https://doi.org/10.1061/JWRMD5.WRENG-5631.
[32] Iannacone L, Sharma N, Tabandeh A, Gardoni P. Modeling time-varying reliability and resilience of deteriorating infrastructure. Reliab Eng Syst Saf 2022;217: 108074. https://doi.org/10.1016/j.ress.2021.108074.
[33] Ester M, Kriegel H-P, Xu X, Sander J. A density-based algorithm for discovering clusters in large spatial databases with noise. In: Proceedings of the 2nd ACM international conference on knowledge discovery and data mining (KDD); 1996. p. 226–31.
[34] National Weather Service, "Weather.gov." Accessed: Mar. 03, 2023. [Online]. Available: https://www.weather.gov/.
[35] C. Pollock, "Texas power almost fully restored and grocery stores will soon be restocked | The Texas tribune", The Texas Tribune. Accessed: Sep. 23, 2022. [Online]. Available: https://www.texastribune.org/2021/02/21/texas-power-outage-grocery-stores-greg-abbott/.
[36] Busby JW, et al. Cascading risks: understanding the 2021 winter blackout in Texas. Energy Res Soc Sci 2021;77:102106. https://doi.org/10.1016/j.erss.2021.102106.
[37] Castellanos S, et al. A synthesis and review of exacerbated inequities from the February 2021 winter storm (Uri) in Texas and the risks moving forward. Prog Energy 2023;5(1):012003. https://doi.org/10.1088/2516-1083/aca9b4.
[38] TCEQ. After-action review of public water systems and winter storm Uri 2022. Accessed: Sep. 23[Online]. Available, https://www.tceq.texas.gov/drinkingwater/after-action-review.
[39] Watson KP, et al. The winter storm of 2021. Hobby school of public affairs. University of Houston; 2021.
[40] United States Environmental Protection Agency, "Analyze trends: EPA/state drinking water dashboard." Accessed: Sep. 23, 2022. [Online]. Available: https://

echo.epa.gov/trends/comparative-maps-dashboards/trends/comparative-maps-dashboards/drinking-water-dashboard.
[41] Montgomery DC. Introduction to statistical quality control. 6th ed. Hoboken, NJ: John Wiley & Sons; 2009.
[42] Seow C. Six sigma for operational excellence. Bradford: Emerald Publishing Limited; 2004.
[43] Rajani B, Kleiner Y, Sink J-E. Exploration of the relationship between water main breaks and temperature covariates. Urban Water J 2012;9(2):67–84. https://doi.org/10.1080/1573062X.2011.630093.
[44] Kwasinski A. Quantitative model and metrics of electrical grids' resilience evaluated at a power distribution level. Energies 2016;9(2):93. https://doi.org/10.3390/en9020093.
[45] Poulin C, Kane MB. Infrastructure resilience curves: performance measures and summary metrics. Reliab Eng Syst Saf 2021;216:107926. https://doi.org/10.1016/j.ress.2021.107926.
[46] Francis R, Bekera B. A metric and frameworks for resilience analysis of engineered and infrastructure systems. Reliab Eng Syst Saf 2014;121:90–103. https://doi.org/10.1016/j.ress.2013.07.004.
[47] Pedregosa F, et al. Scikit-learn: machine learning in Python. J Mach Learn Res 2011;12(85):2825–30.
[48] Schubert E, Sander J, Ester M, Kriegel HP, Xu X. DBSCAN revisited, revisited: why and how you should (still) use DBSCAN. ACM Trans Database Syst 2017;42(3):1–21. https://doi.org/10.1145/3068335.
[49] Ting KM. Precision and Recall. In: Sammut C, Webb GI, editors. Encyclopedia of machine learning. Boston, MA: Springer US; 2010. p. 781. https://doi.org/10.1007/978-0-387-30164-8_652. editors.
[50] Nielsen-Gammon JW. The 2011 Texas drought. Tex Water J 2012:59–95. https://doi.org/10.21423/TWJ.V3I1.6463.
[51] Golbeck J. Chapter 3—Network structure and measures. In: Golbeck J, editor. Analyzing the social web. Boston: Morgan Kaufmann; 2013. p. 25–44. https://doi.org/10.1016/B978-0-12-405531-5.00003-1. editor.
[52] Austin Water, "Understanding the Drought", 2015. Accessed: Jan. 10, 2023. [Online]. Available: https://www.austintexas.gov/page/drought-response.
[53] Fernandez M. Sacrifices and restrictions as central Texas town copes with drought. The New York Times; 2011. Accessed: Jan. 10, 2023. [Online]. Available, https://www.nytimes.com/2011/09/07/us/07drought.html.
[54] United States Environmental Protection Agency, "Saving water in Texas", 2016, Accessed: Jan. 10, 2023. [Online]. Available: www.epa.gov/watersense.